Int. J. Therm. Sci. (1999) 38, 492–500

Prediction of thermal protection of walls by blowing with different fluids

Jérôme Bellettre, Françoise Bataille, André Lallemand*

Centre de thermique de Lyon, Upres A CNRS 5008, Insa de Lyon, 20 av. Albert-Einstein, 69621 Villeurbanne cedex, France

(Received 26 May 1998, accepted 25 October 1998)

Abstract — This work concerns the modelling of heat and mass transfer in the boundary layer and inside a plane porous plate which is below a hot fluid flow and submitted to cold fluid blowing. A preliminary study of the heat transfer rates in the boundary layer without blowing permits us to validate, comparing with experimental results, the RNG $k-\varepsilon$ model. The RNG $k-\varepsilon$ model, with kinematic and thermal laws for the wall, linked with a model of blowing, is then used to study the heat and mass transfer rates at the wall when the main flow and the injected fluids are of the same species – air – but at different temperatures. The comparison between calculated friction factors, Stanton numbers and published results confirms the validity of our model. We also show the strong influence of the injection rate on the thermal convective coefficient of the wall. In the last part, results on cooling by blowing with water vapour in a main flow of air are given. Comparisons of the evolution of Stanton numbers and friction factors show that blowing with water vapour is more efficient than air injection in terms of momentum transfer and thermal protection of walls. © Elsevier, Paris.

turbulent boundary layer / convection / blowing / heat transfer coefficient / water vapour / air

Résumé — Prédiction de la protection thermique de parois par effusion de différents fluides. Ce travail concerne la modélisation des transferts de masse et de chaleur dans la couche limite et à l'intérieur d'une paroi poreuse plane soumise à un écoulement pariétal d'un fluide chaud et à l'effusion d'un fluide froid. Une étude préliminaire des transferts en couche limite sans effusion permet de valider, à partir de résultats expérimentaux, le modèle RNG $k-\varepsilon$ pour l'écoulement turbulent. Le modèle RNG $k-\varepsilon$ avec les lois de paroi cinématique et thermique, couplé avec un modèle d'effusion à travers une paroi poreuse, est ensuite mis en pratique pour étudier les transferts de chaleur et de quantité de mouvement à la paroi lorsque les écoulements pariétal et d'effusion concernent un fluide identique – de l'air – à des températures différentes. La comparaison des coefficients de frottement et des nombres de Stanton calculés et fournis par la littérature confirme la validité de notre modélisation. On montre également la forte influence du taux d'effusion sur le coefficient de convection thermique à la paroi. Dans la dernière partie, les résultats concernant un refroidissement par de la vapeur d'eau dans un écoulement pariétal d'air sont donnés. La comparaison de l'évolution des nombres de Stanton et des coefficients de frottement montre que l'effusion de vapeur d'eau est plus efficace que celle d'air, tant pour le transfert de quantité de mouvement que pour la protection thermique de la paroi. © Elsevier, Paris.

couche limite turbulente / convection / injection / coefficient d'échange thermique / vapeur d'eau / air

Nomenclature

A	Van Driest constant ($A = 26$)	
B	blowing factor ($B = F/St$)	
B_f	blowing factor ($B_f = 2F/C_f$)	
C	mass fraction (mean value)	
C_f	friction factor $\left(\frac{C_f}{2} = \frac{\tau_w}{\rho_e U_e^2}\right)$	
c'	mass fraction fluctuation	
c_p	specific heat	$J\cdot kg^{-1}\cdot K^{-1}$
D	diffusive coefficient	$m^2\cdot s^{-1}$
E	friction constant ($E = 9.0$ for a smooth wall)	
F	injection rate ($F = (\rho U_2)_w/(\rho U_1)_e$)	
H	enthalpy (mean value)	$J\cdot kg^{-}1$
h	convective heat transfer coefficient	$W\cdot m^{-2}\cdot K^{-1}$
h'	enthalpy fluctuation	$J\cdot kg^{-1}$
I_u	longitudinal turbulence intensity	
J	diffusion flux	$kg\cdot m^{-2}\cdot s^{-1}$
k	turbulent kinetic energy	$m^2\cdot s^{-2}$
P	pressure	Pa

* Correspondence and reprints.
a.lal@cethil.insa-lyon.fr

Pr Prandtl number ($Pr = \mu c_p/\lambda$)
q heat flux ..... $W{\cdot}m^{-2}$
Re_L Reynolds number ($Re_L = \rho U_{1e} L/\mu$)
St Stanton number $\left(St = \dfrac{h}{\rho U_{1e} c_p}\right)$
T temperature ..... K
U velocity (mean value) ..... $m{\cdot}s^{-1}$
u' Velocity fluctuation ..... $m{\cdot}s^{-1}$
U^* friction velocity $\left(U^* = \sqrt{\dfrac{\tau_w}{\rho}}\right)$ ..... $m{\cdot}s^{-1}$
x spatial coordinate ..... m
y^+ dimensionless coordinate $\left(y^+ = \dfrac{\rho U^* x_2}{\mu}\right)$

Greek letters

Δ Enthalpy thickness $\left(= \displaystyle\int_0^\infty \frac{\rho C_p U_1}{\rho_e C_{p_e} U_{1e}} \frac{T - T_e}{T_w - T_e}\, dx_2\right)$ .... m
δ_{ij} Kronecker symbol
ε turbulent kinetic energy dissipation rate $m^2{\cdot}s^{-3}$
κ Von Karman constant ($\kappa = 0.44$)
λ Thermal conductivity ..... $W{\cdot}m^{-1}{\cdot}K^{-1}$
μ dynamic viscosity ..... $kg{\cdot}m^{-1}{\cdot}s^{-1}$
ν kinematic viscosity ..... $m^2{\cdot}s^{-1}$
θ momentum thickness $\left(= \displaystyle\int_0^\infty \frac{\rho U_1}{\rho_e U_{1e}} \left(1 - \frac{U_1}{U_{1e}}\right) dx_2\right)$ .... m
ρ density ..... $kg{\cdot}m^{-3}$
σ_h turbulent Prandtl number
σ_m turbulent Schmidt number
τ shear stress $= \mu\left(\dfrac{\partial U_1}{\partial x_2}\right)_w$ ..... Pa

Subscripts

0 without blowing
1 longitudinal direction
2 vertical direction
a air
e main flow
i,j i, j directions
mol molecular
p close to the wall (i.e. at the first node)
t turbulent
v vapour
w on the wall

1. INTRODUCTION

Wall cooling is an essential element in the protection of surfaces exposed to high temperatures. Different techniques can be used for protecting surfaces. The most frequently used is discrete injection where the wall is perforated and coolant fluid flows on the wall surface [1]. Another possibility is the ablation for which a solid thermally degradable material is added on the wall. However, the most efficient way to prevent degradations of materials is blowing (continuous injection). In this case, the surface of walls are porous, which can also present advantages (weight). Many parameters can influence the cooling system: the cooling fluid can be chemically different from the main flow; the injection rate can vary and changes the behaviour of the boundary layer; evaporation or sublimation can also be used to increase the cooling efficiency.

In this paper, we are concerned with the study of turbulent boundary layers subjected to blowing through a porous plate. In the literature, to take blowing into account, modified laws of wall were used ([2, 3]), and modified mixing length models were developed ([4, 5]). We can also quote the works on the modified low Reynolds models [6, 7]. In this study, we point out the physical phenomena involved in the blowing and we model the effects on the boundary layer. The results of our modeling are compared with an experimental study conducted in the test channel of our laboratory [8] permitting the validation of the numerical results. Furthermore, data from the literature are used.

In the present work, blowing with air, where the coolant fluid is the same as the main flow, is first investigated. Then, blowing with water vapour is studied. In both cases, we are interested in the fluid dynamic (velocity profile, friction factor) and thermal aspects (temperature profile, Stanton number).

2. PRESENTATION OF THE STUDY AND GOVERNING EQUATIONS

The equations for the mean flow are the continuity, momentum and energy equations where the Reynolds decomposition is applied (equations (1)–(3)). Furthermore, when the case of injection with different species (air-steam) is treated, a vapour mass budget (4) is added.

$$\frac{\partial \rho U_j}{\partial x_j} = 0 \tag{1}$$

$$\frac{\partial}{\partial x_j}(\rho U_i U_j) = -\frac{\partial P}{\partial x_i} + \frac{\partial}{\partial x_j}\left(\mu\left[\frac{\partial U_i}{\partial x_j} + \frac{\partial U_j}{\partial x_i}\right] - \frac{2}{3}\mu\frac{\partial U_i}{\partial x_i} - \rho\overline{u_i' u_j'}\right) \tag{2}$$

$$\frac{\partial}{\partial x_j}(\rho U_j H) = \frac{\partial}{\partial x_j}\left(\lambda\frac{\partial T}{\partial x_j}\right) - \frac{\partial}{\partial x_j}\left(\rho\overline{u_j' h'}\right) + U_j\frac{\partial P}{\partial x_j} - \frac{\partial}{\partial x_j}\left((H_v - H_a)\, J\right) \tag{3}$$

$$\frac{\partial}{\partial x_j}(\rho U_j C) = -\frac{\partial}{\partial x_j}(J) \tag{4}$$

with $J = -\rho D \dfrac{\partial C}{\partial x_j} + \rho \overline{c' u'_j}$

In these equations, U, H and P are the mean values of the mixture velocity, enthalpy and pressure, u' and h' the velocity and enthalpy fluctuations. ρ represents the fluid density, μ the dynamic viscosity, λ the thermal conductivity for the mixture. For the vapour species, J is the diffusion flux, H_v is the mean value of the vapour enthalpy, C the local mass fraction, c' its fluctuation and D the diffusive coefficient in air. H_a is the mean value of the air enthalpy. Furthermore, ρ, μ and λ are temperature- and concentration-dependent; D is temperature-dependent according to tabulated values.

The experimental configuration of the study is illustrated in *figure 1*. In the wind tunnel, the floor is first constituted as an impermeable wall (1.30 m), then of a porous plate (30 cm) where the cold fluid is injected. The main flow has a longitudinal velocity, U_1 (10 m·s^{-1}), and a longitudinal turbulence intensity, I_u, of 1 %. The Reynolds number is high enough to have a turbulent boundary layer before the porous plate ($Re_{x1} = 856\,000$). Furthermore, this boundary layer of the developing turbulent flow is two-dimensional. We note x_1 the longitudinal coordinate and x_2 the vertical one (the origin being in the bottom left corner of the channel).

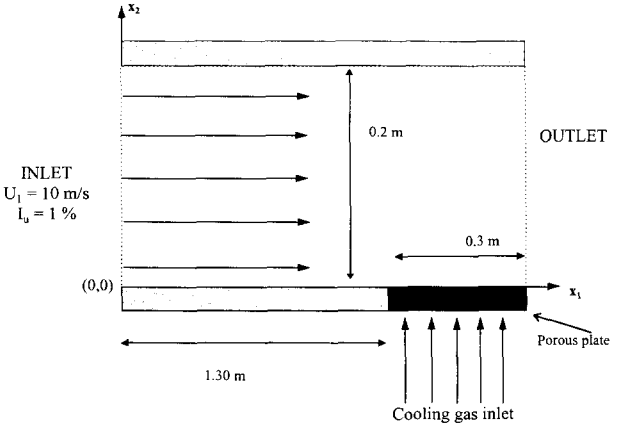

Figure 1. Configuration of the study.

3. TURBULENCE MODEL AND BLOWING

In this work, the main idea is to use a classical model of turbulence and to model the blowing through the porous plate. Consequently, to close the system described above, we tested and selected a model of turbulence in a case without blowing. For this study, we have considered the Renormalisation Group $k-\varepsilon$ model (RNG). The RNG $k-\varepsilon$ model extends the classical prediction of the turbulent viscosity. Nevertheless, the assumptions and the improvement of this concept are not stated here and only the governing equations are presented. More detail can be found in references [9–11]. The turbulent Reynolds stresses appearing in the main flow equations are modelled using a turbulent viscosity ν_t:

$$\overline{u'_i u'_j} = -\nu_t \left(\frac{\partial U_i}{\partial x_j} + \frac{\partial U_j}{\partial x_i}\right) + \frac{2}{3}\nu_t \frac{\partial U_i}{\partial x_i}\delta_{ij} + \frac{2}{3} k \delta_{ij} \tag{5}$$

$$\overline{u'_j h'} = -\frac{\nu_t}{\sigma_h}\frac{\partial c_p T}{\partial x_j} \tag{6}$$

$$\overline{c' u'_j} = -\frac{\nu_t}{\sigma_m}\frac{\partial C}{\partial x_j} \tag{7}$$

with $\sigma_h = 0.7$ (turbulent Prandtl number) and $\sigma_m = 1$ (turbulent Schmidt number). ν_t is determined by k, the turbulent kinetic energy and ε, the dissipation rate of k, according to the relation (8).

$$\nu_t = C_\mu \frac{k^2}{\varepsilon} \tag{8}$$

with $C_\mu = 0.0845$.

k and ε are obtained from the solution of their respective model transport equations (9) and (10).

$$\frac{\partial(\rho U_j k)}{\partial x_j} = \frac{\partial}{\partial x_j}\left[\alpha_k \rho \nu_{eff}\frac{\partial k}{\partial x_j}\right] + \mu_t\left(\frac{\partial U_i}{\partial x_j} + \frac{\partial U_j}{\partial x_i}\right)\frac{\partial U_i}{\partial x_j} - \rho\varepsilon \tag{9}$$

$$\frac{\partial(\rho U_j \varepsilon)}{\partial x_j} = \frac{\partial}{\partial x_j}\left(\alpha_\varepsilon \rho \nu_{eff}\frac{\partial \varepsilon}{\partial x_j}\right) + C_{\varepsilon 1}\frac{\varepsilon}{k}\mu_t\left(\frac{\partial U_i}{\partial x_j} + \frac{\partial U_j}{\partial x_i}\right)\frac{\partial U_i}{\partial x_j} - C_{\varepsilon 2}\rho\frac{\varepsilon^2}{k} - R \tag{10}$$

with $\alpha_k = \alpha_\varepsilon = 1.39$, $C_{\varepsilon 1} = 1.42$, $C_{\varepsilon 2} = 1.68$ and $\nu_{eff} = \nu_{mol}\left(1 + \sqrt{\dfrac{\nu_t}{\nu_{mol}}}\right)^2$ (ν_{mol} being the molecular kinetic viscosity). Finally,

$$R = \frac{\rho C_\mu \eta^3 \left(1 - \dfrac{\eta}{4.38}\right)}{1 + 0.012\,\eta^3}\frac{\varepsilon^2}{k}$$

where $\eta = S\,k/\varepsilon$, $S = (2 S_{ij} S_{ij})^{1/2}$ and

$$S_{ij} = \frac{1}{2}\left(\frac{\partial U_j}{\partial x_i} + \frac{\partial U_i}{\partial x_j}\right)$$

3.1. Boundary conditions on impermeable plate

In order to take into account the near wall effect, the Launder and Spalding logarithmic-law of the wall treatment (11) is used under the condition of equilibrium [12]:

$$\frac{U_1}{U^*} = \frac{1}{\kappa} \ln(Ey^+), \text{ for } 11 < y^+ < 50 \qquad (11)$$

where $U^* = \sqrt{\frac{\tau_w}{\rho_w}}$, τ_w is the wall shear stress, κ is the von Karman's constant and E is an empirical constant set equal to 9.0 (smooth wall). y^+ is the dimensionless coordinate defined by relation (12):

$$y^+ = \frac{\rho U^* x_2}{\mu} = \frac{\rho C_\mu^{1/4} k_p^{1/2} x_2}{\mu} \qquad (12)$$

The near wall value of the kinetic energy (k_p) is calculated by solving the complete transport equation for k with a zero normal gradient assumed at the wall. The boundary condition for $\varepsilon(\varepsilon_p)$ is given by the equilibrium assumption [12] implying $\varepsilon_p = \frac{C_\mu^{3/4} k_p}{\kappa x_{2p}}$ (x_{2p} being the vertical coordinate of the nearest point of the wall).

Thermal boundary conditions on the wall are modelled using the Launder and Spalding [12] logarithmic-law of the wall:

$$\frac{\lambda(\Delta T/x_{2p})}{q} = \frac{1}{\kappa y^+} \frac{\sigma_h}{Pr} \ln(Ey^+) + \frac{1}{y^+} \left(\frac{\sigma_h}{Pr}\right)^{5/4} \frac{\pi/4}{\sin(\pi/4)} \left(\frac{A}{\kappa}\right)^{1/2} \left(\frac{Pr}{\sigma_h} - 1\right) \qquad (13)$$

where q is the heat transfer at the wall, $\Delta T = T_w - T_p$ (T_w is the wall temperature and T_p is the near wall temperature), Pr the fluid Prandtl number, σ_h the turbulent Prandtl number (0.85 near the wall) and A the van Driest constant ($A = 26$). T_w can be either fixed or calculated according to the external heat transfer boundary conditions.

3.2. Model of the blowing

For this model, we represent the porous plate by a succession of two different kinds of elements. The first one is similar to a wall which is governed by the classical laws of the wall, the second one is considered as a source of fluid. This flow is laminar, at a given temperature and velocity taking into account the cross section inside the plate. Consequently, the boundary layer is subjected to blowing results in the mixing of two flows (main flow and injected flow). Physical arguments and details on this modelling can be found in Bellettre et al. [13].

3.3.Numerical method

The numerical technique used in the present investigation is a finite volume approach with quadrilateral control volumes and structured meshes. The diffusion terms are discretized according to a central difference method and a power law scheme is used for the convective terms. Pressure velocity coupling is calculated with the SIMPLE cell-centered scheme [14].

For all the calculations, we used a cartesian grid. In the longitudinal direction, the grid is linear with more concentration on the porous area than on the impermeable plates (*figure 2*). A sensitivity study showed that between 1 and 5 mm the discrete step on the porous plate has no effect on the calculations. In the vertical direction, the grid can be either linear or have a geometrical progression. We observed that the numerical results are independent of the grid type and of the vertical space step (tested between 0.75 and 3 mm) for a linear grid. In the present work, the number of grid nodes is 17 000. The laws of the wall (11) and (13) are used only for first point over the wall (with $11 < y_p^+ < 50$).

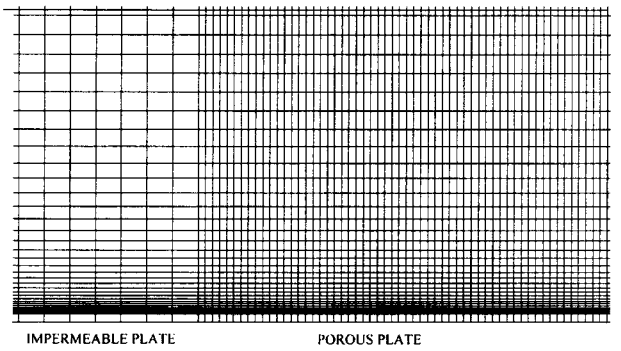

Figure 2. Computational grid.

Finally, we tested the convergence of the calculations according to two criteria: all the normalized residuals have to be less than 10^{-4} and supplementary iterations do not change the calculation results.

4. PRELIMINARY STUDY

The RNG $k - \varepsilon$ model is used to simulate the turbulent flow in the configuration shown in *figure 1*, but without injection. In order to validate this model, we used experimental velocities measured by laser- Doppler anemometry in our subsonic test channel and results from the literature. The test channel is described in *figure 3* and more details can be found in Rodet et al. [8].

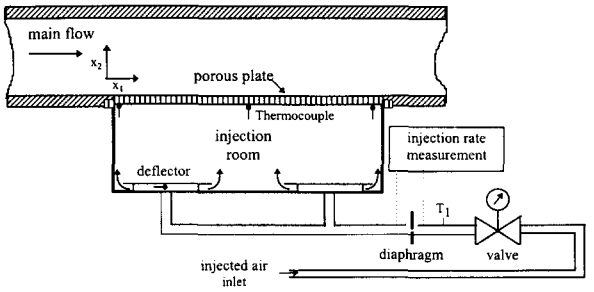

Figure 3. Test channel.

Longitudinal velocities in a boundary layer at $Re_{x1} = 856\,000$ are computed. Calculations from the model are compared with experimental data [8]. The results are shown in *figure 4*. It is notable that the RNG $k-\varepsilon$ calculations and experimental data match very well.

To characterise the boundary layer, we calculated the friction factor using the momentum thickness (θ) defined by $\theta = \int_0^\infty \frac{\rho U_1}{\rho_e U_{1e}} \left(1 - \frac{U_1}{U_{1e}}\right) dx_2$. In the case of a turbulent flow, on an impermeable plate, Simpson et al. [15] and Andersen et al. [16] proposed the relations (14) and (15). The friction factor without blowing, C_{f0}, is obtained using correlations which take into account the Reynolds number based on the momentum thickness. The coefficients of these two correlations have been experimentally determined. Nevertheless, the results of Simpson et al. [15] seem to be too high according to [17]:

$$\frac{C_{f0}}{2} = a\, Re_\theta^{-0.25} \quad \text{with } a = 0.013 \qquad (14)$$

$$\text{with } a = 0.012 \qquad (15)$$

Figure 5 gives the comparison between the correlations of Simpson et al. [15], Andersen et al. [16] and the results obtained with the RNG $k-\varepsilon$ model. In the RNG $k-\varepsilon$ case, the friction factor is determined according

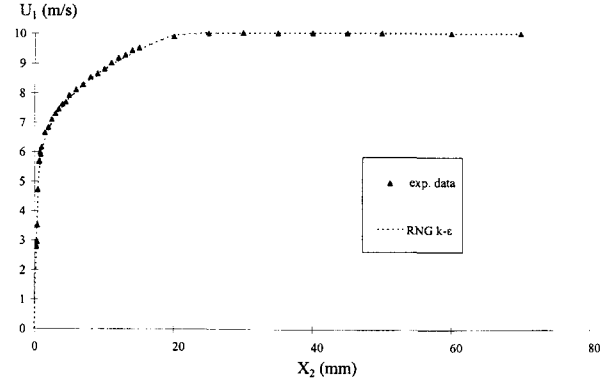

Figure 4. Experimental and calculated velocities without blowing.

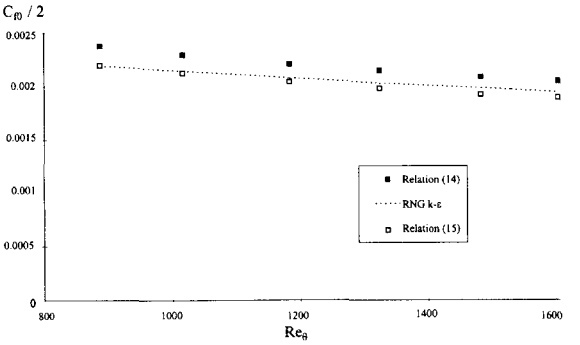

Figure 5. Friction factors for Re_θ varying from 900 to 1 600.

to the relation : $\frac{C_{f0}}{2} = \frac{\rho_w}{\rho_e}\left(\frac{U^*}{U_e}\right)^2$ with $U^* = C_\mu^{1/4} k_p^{1/2}$ (deduced from equation (12)). Furthermore, in relations (14) and (15), the Reynolds number based on momentum thickness is computed by integrating the numerical profile of longitudinal velocity in the boundary layer. We can notice that the results of Andersen's correlation are very close to our model.

To calculate the thermal transfer with Stanton number, we used the relation (16) proposed by Whitten et al. [18], which involves the Reynolds number based on the enthalpy thickness Δ, defined by $\Delta = \int_0^\infty \frac{\rho U_1}{\rho_e U_{1e}} \frac{T - T_e}{T_w - T_e} dx_2$, and which has been obtained for a weak temperature difference between the main flow and the wall:

$$St_0 = 0.0128\, Re_\Delta^{-0.25}\, Pr^{-0.5} \qquad (16)$$

We can see in *figure 6* that the results of the RNG $k-\varepsilon$ model ($St = \frac{q_w}{\rho_e (T_w - T_e) U_e c_p}$ and q_w is calculated according the relation (13)) are in good agreement with the relation of Whitten et al. [18], where the enthalpy thickness is calculated by integrating the velocity and temperature profiles in the boundary layer.

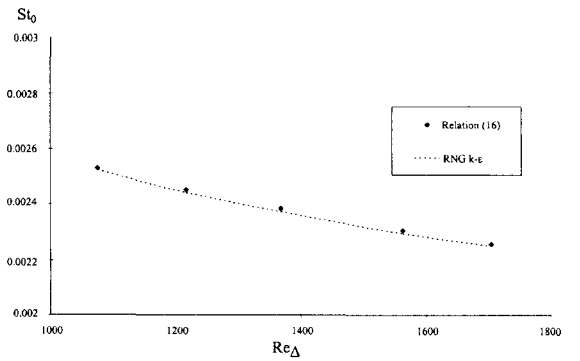

Figure 6. Stanton numbers for Re_Δ varying from 1 000 to 1 700.

According to all these results without blowing, the RNG $k-\varepsilon$ model seems to be very well suited to our flow configuration. In the framework of our study, we could test other, more elaborate models [19] for the turbulent flows but it is not the objective of the present work. Now, we will use the RNG $k-\varepsilon$ model for the main flow and investigate the study of the turbulent boundary layer with blowing.

5. RESULTS WITH AIR

Initially, we considered injection with air, that is to say that the main flow and the injected flow are same species.

In *figure 7*, we plot the numerical longitudinal velocity profile without injection and with different injection rate ($F = (\rho U_2)_w/(\rho U_1)_e$) varying from 0 to 1.5 %. We can observe that the flow is affected by the injection and this leads to an important increase of the boundary layer thickness when the injection rate increases.

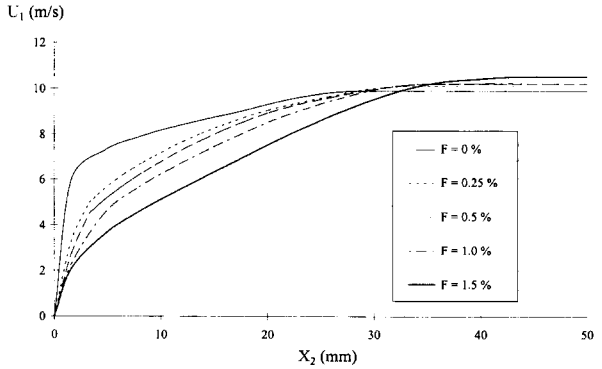

Figure 7. Velocity profiles for $0 \leq F \leq 1.5$ % at $x_1 = 1.55$ m.

In *figure 8*, the numerical temperature profile is plotted for different injection rates in the case where the main flow temperature is 200 °C and the temperature of the injected fluid is 100 °C. We can observe that there is an increase of the thermal boundary layer thickness. This increase is particulary important for high injection rates. As a result, when blowing occurs, the heat transfer is greatly reduced and permits an efficient protection of the porous plate.

In this study, we are interested in the friction factor when blowing occurs. The friction factor is calculated using Simpson et al. [15] correlation (17), where the friction factor without blowing, C_{f0}, is given by Andersen et al. [16] relation (15):

$$\left.\frac{C_f}{C_{f0}}\right|_{Re_\theta} = \left[\frac{\ln(1+B_f)}{B_f}\right]^{0.7} \qquad (17)$$

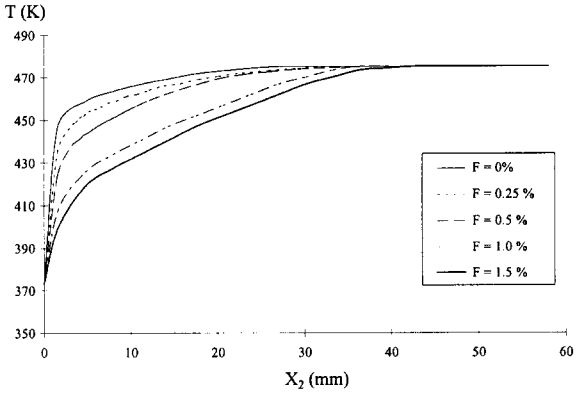

Figure 8. Temperature profiles for $0 \leqslant F \leq 1.5$ % at $x_1 = 1.55$ m.

where $B_f = 2F/C_f$, $0.2 < 1 + B_f < 65$ and θ is calculated by numerical data integration.

The evolution of the friction factor[1] as a function of the injection rate is shown in *figure 9*. The classical decrease in the friction factor with the injection rate is found and we note that the results are close to experimental data. Comparisons are given here for equivalent boundary layer configurations, i.e. experimental Reynolds numbers based on momentum thickness are equal to those of our simulations. Furthermore, the friction factor, determined as in section 4 has been compared with results of correlations (17). We observe in *figure 10* that the two curves are very similar.

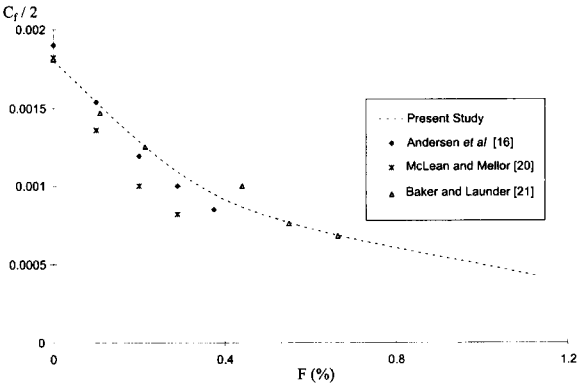

Figure 9. Friction factors for different injection rates.

The Stanton number permits calculation of the heat transfer coefficient, h, between main flow and the wall. Now, we determined the Stanton number for different

[1] In all the study (without and with blowing), the friction factor is relative to the average wall shear stress on the total surface of the porous plate.

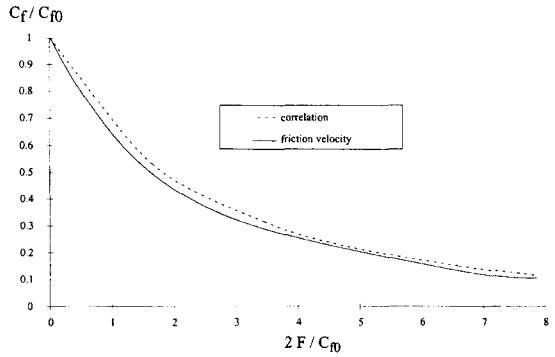

Figure 10. Friction factors calculated with the correlation or the friction velocity.

injection rates using the correlation of Whitten et al. [18] (equation (18)).

$$\left.\frac{St}{St_0}\right|_{Re_\Delta} = \left[\frac{\ln(1+B)}{B}\right]^{1.25} (1+B)^{0.25} \qquad (18)$$

with $St_0 = 0.0128\, Re_\Delta^{-0.25}\, Pr^{-0.5}$, $B = F/St$ and Δ calculated by numerical data integration.

We can observe in *figure 11* that we obtained a very good agreement between our calculations and results from the literature. Plotted, in *figure 12*, is the convective heat transfer coefficient between the porous plate and the main flow. We can note that, for an injection rate of 1 %, the coefficient is reduced by about 80 %, showing the high efficiency of this kind of protection.

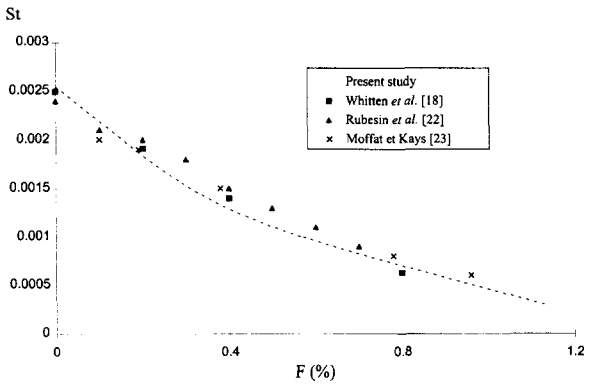

Figure 11. Stanton numbers for different injection rates.

6. RESULTS WITH WATER VAPOUR

After considering the case where the main flow and the injected fluid are of same species (air), we are here interested in water vapour injection with a main flow of

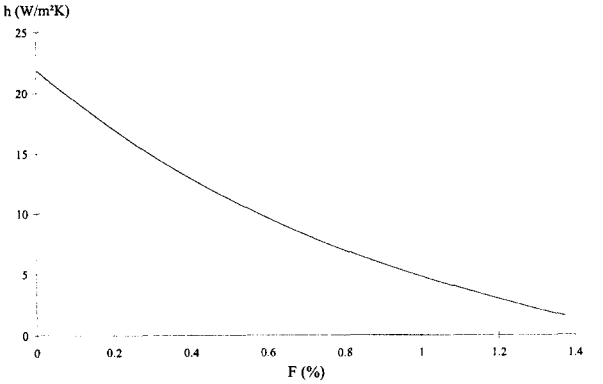

Figure 12. Convective heat transfer coefficients for different injection rates.

air. The temperature of the main flow is 200 °C and the injected fluid temperature is 100 °C. This last boundary condition could correspond to a liquid-vapour interface of water under a 100 kPa pressure level.

The numerical velocity and temperature profiles are plotted for the injection of air and the injection of water vapour (the injection rate being equal to 0.5 %) on *figures 13* and *14*. We can see that the velocity profiles with air and steam injection are very close and that there is no notable difference for this injection rate. This result is in good agreement with experimental data obtained for freon injection and air injection which show the similarity of the two velocity profiles for a fixed injection rate [21]. In *figure 14*, we note that the temperature in the boundary layer is lower in the case of water injection. Consequently, the thermal protection by water vapour injection should be more efficient compared to air injection.

It is interesting to calculate and to compare Stanton number and friction factor for injection of air and water. For both cases, we used the correlations given in section 5 (equations (17) and (18)) and we compared the results with the numerical work of Landis and

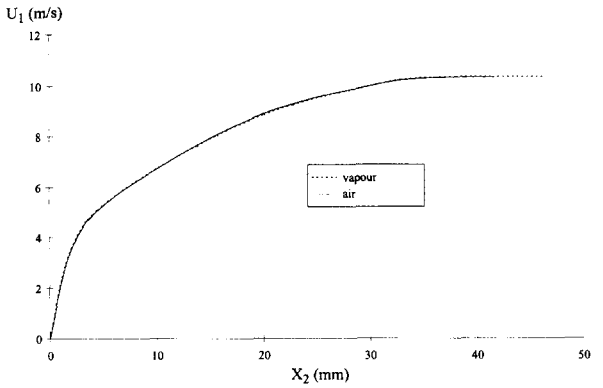

Figure 13. Velocity profiles for air or vapour injection ($F = 0.5$ %, $x_1 = 1.55$ m).

Mills [5]. In *figure 15*, the ratio of the Stanton number for water vapour to the Stanton number for air is plotted for different injection rates. We can see that the Stanton number with water injection is lower than the Stanton number with air injection, particularly when the injection rate increases. Furthermore, we can observe that the present results are close to the Landis and Mills [5] values which permit us to validate the use of the Whitten et al. [18] correlation, initially established only with air. Nevertheless, since between 100 °C and 200 °C, the thermal conductivity of water is almost equal to that of air, we could suppose that this correlation stays valid for air and steam. The ratio of the friction factor for water vapour to the friction factor for air at different injection rates was studied in [24]. The results using Simpson et al. [15] correlation are not satisfactory when comparing with Landis and Mills [5] values. It seems that, in the case of water vapour, it is not possible to use the Simpson et al. [15] correlation established for air. An explanation could be that the difference of the dynamic viscosity (the dynamic viscosity of steam is about half the air one (at 100 °C)) is not taken into account in the correlation, leading to an overestimation of the friction factor.

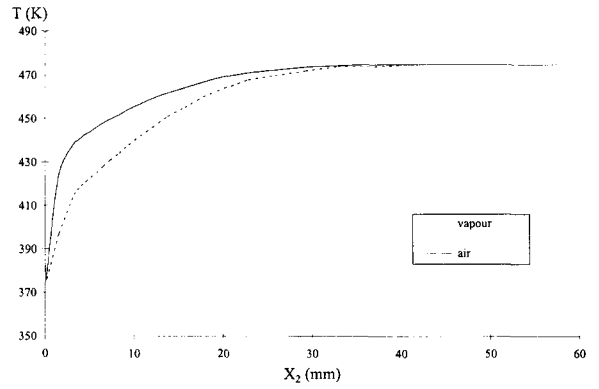

Figure 14. Temperature profiles for air or vapour injection ($F = 0.5$ %, $x_1 = 1.55$ m).

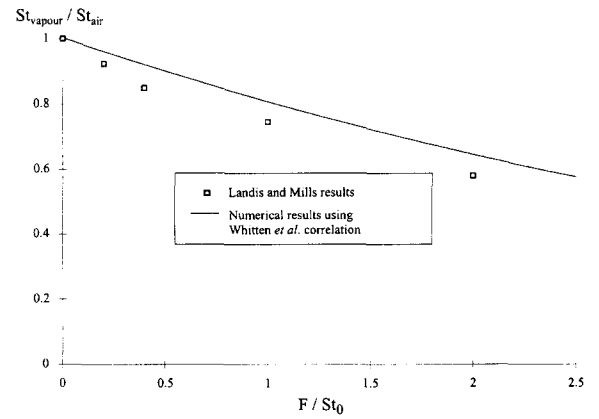

Figure 15. Ratio of Stanton numbers.

To check our numerical results, we calculated the friction factor using the friction velocity, U^*, of the law of the wall (11), which is calculated for each solid element of the porous plate ($U^* = C_\mu^{1/4}\, k_p^{1/2}$). According to Landis and Mills [5], it seems that the wall shear stress is mostly determined by the log region of the boundary layer and, in this region, the present k_p values are calculated taking into account the real property of the mixture (viscosity and density). We again compared with Landis and Mills [5] data. In *figure 16*, we can see that a rather good agreement is obtained and that the friction factor for the water vapour is lower than for the air.

The more important decrease of friction coefficients by blowing with water vapour instead of air could be interesting for applications where drag forces must be reduced.

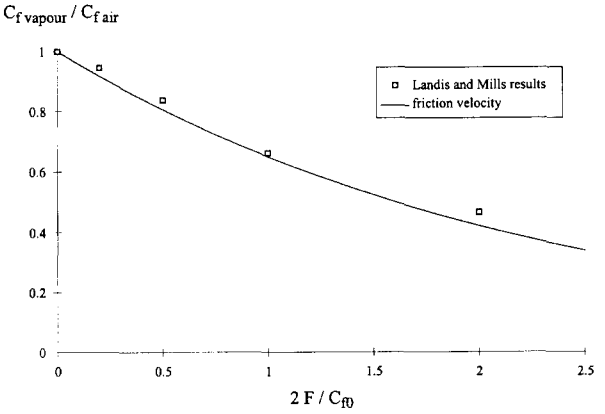

Figure 16. Ratio of friction factors (using friction velocity).

7. CONCLUSION

In order to study the thermal protection of porous walls below a hot turbulent boundary layer, a new model of blowing is used. The dynamic and thermal aspect of a turbulent boundary layer submitted to blowing is studied. The thermal protection of walls using injection of air and water vapour is investigated. It has been found that the friction factors and Stanton numbers are modified when blowing occurs. The modifications are different when the injected fluid is not of the same species as the main flow. In the case of steam, the friction factors and Stanton numbers are found lower than in the case of air injection, specially when the injection rate increases.

A more complete study with liquid injection including phase change in the porous media would permit us to precisely evaluate the interest of using liquid instead of gas.

REFERENCES

[1] Carcasci C., Facchini B., A numerical procedure to design internal cooling of gas turbine stator blades, Rev. Gén. Therm 35 (1996) 257–268.

[2] Stevenson T.N., Inner region of transpired turbulent boundary layers, AIAA J. 6 (1968) 553–554.

[3] Simpson R.L., Characteristics of turbulent boundary layers at low Reynolds Numbers with and without transpiration, J. Fluid Mech. 42 (1970) 769–802.

[4] Kays W.M., Heat transfer to the transpirated turbulent boundary layer, Int. J. Heat Mass Tran. 15 (1972) 1023–1044.

[5] Landis R.B., Mills F., The calculation of turbulent boundary layers with foreign gas injection, Int. J. Heat Mass Tran. 15 (1972) 1905–1932.

[6] Campolina França G.A., Tedeschi G., Lallemand A., Turbulent incompressible flow within a channel with transpiration: solution of the coupled problem porous wall – main flow, in: 13th Brasilian Congress and 2nd Iberian American Congress of Mechanical Engineering, Belo Horizonte, Brasil, 1995, 4 p.

[7] Campolina França G.A., Pagnier P., Lallemand A., Simulation des transferts de masse et de chaleur par modèlisation à bas nombres de Reynolds dans un écoulement à effusion locale en canalisation, Rev. Gén. Therm. 37 (1998) 205–222.

[8] Rodet J.-C., Campolina Franca G.A., Pagnier P., Morel R., Lallemand A., Étude en soufflerie thermique du refroidissement de parois poreuses par effusion de gaz, Rev. Gén. Therm. 37 (1998) 123–136.

[9] Yakhot V., Orszag S.A., Renormalization Group Analysis of Turbulence, I. Basic Theory, J. Sci. Comput. 1 (1986) 1–51.

[10] Yakhot V., Smith L.M., The renormalization group, the e expansion, and derivation of turbulence models, J. Sci. Comput. 7 (1992) 35.

[11] Zhou Y., McComb D.W., Vahala G., Renormalization group (RG) in turbulence: historical and comparative perspective, Icase report 97–36, Langley, 1997.

[12] Launder B.E., Spalding D.B., The numerical computation of turbulent flow, Comput. Method. Appl. M. 3 (1974) 269–288.

[13] Bellettre J., Bataille F., Lallemand A., A study of a turbulent boundary layer with injection, in: ASME fluids engineering division summer meeting, Symposium on separated and complex flows, Vancouver, Canada, 1997, 8 p.

[14] Patankar S.V., Numerical Heat Transfer and Fluid Flow, Hemisphere Publishing Corp., Washington, 1980.

[15] Simpson R.L., Moffat R.J., Kays W.M., The turbulent boundary layer on a porous plate: experimental skin friction with variable injection and suction, Int. J. Heat Mass Tran. 12 (1969) 771–789.

[16] Andersen P.S., Kays W.M., Moffat R.J., Experimental results for the transpired turbulent boundary layer in an adverse pressure gradient, J. Fluid Mech. 69 (1975) 353–375.

[17] Squire L.C., The constant property turbulent boundary layer with injection; a reanalysis of some experimental results, Int. J. Heat Mass Tran. 13 (1970) 939–942.

[18] Whitten D.G., Moffat R.J., Kays W.M., Heat transfer to a turbulent boundary layer with non-uniform blowing and surface temperature, in: Proceeding of the Fourth International Heat Transfer Conference, Versailles, France, 1970, Paper FC 8.8, 12 p.

[19] Younis B.A., Speziale C.G., Clark T.T., A non linear algeabric model for the turbulent scalar fluxes, in: International Conference on Turbulent Heat Transfer, San Diego, USA, 1996, 11 p.

[20] Mc Lean J.D., Mellor G.L., The transpired turbulent boundary layer in an adverse pressure gradient, Int. J. Heat Mass Tran. 15 (1972) 2353–2369.

[21] Baker R.J., Launder B.E., The turbulent boundary layer with foreign gas injection. I. Measurement in zero pressure gradient, Int. J. Heat Mass Tran. 17 (1974) 275–291.

[22] Rubesin M.W., Inouye M., Parikh P.G., Forced convection, external flows, in: Handbook of heat transfer, Fundamentals, 2nd ed., McGraw-Hill Inc., New York, 1985.

[23] Moffat R.J., Kays W.M., A review of turbulent-boundary-layer heat transfer research at Stanford, 1958-1983, Adv. Heat Transfer 16 (1984) 241–365.

[24] Bellettre J., Bataille F., Lallemand A., Blowing with gas or water, in: 11th symposium on Turbulent Shear Flows, Grenoble, France, 1997, vol. 3, pp. P3.1–P3.5.